

---

## Alpha Heating and Burning Plasmas in Inertial Confinement Fusion

In inertial confinement fusion<sup>1</sup> (ICF), a shell of cryogenic deuterium (D) and tritium (T) ice is imploded at high velocities (300 to 400 km/s) and low entropy to achieve high central temperatures and high areal densities.<sup>2</sup> The final fuel assembly consists of a relatively low-density (30- to 100-g/cm<sup>3</sup>), high-temperature (5- to 10-keV) core—the hot spot—surrounded by a dense (300- to 1000-g/cm<sup>3</sup>), cold (200- to 500-eV) fuel layer—the compressed shell. Alpha particles are produced from the D + T fusion reactions with an energy  $\varepsilon_\alpha = 3.5$  MeV and slow down primarily through collisions with the plasma electrons. The alpha-heated electrons transfer part of their energy to the D and T ions, thereby increasing the fusion-reaction rate. The process of depositing alpha energy inside the hot spot of a compressed ICF capsule is called *alpha heating*. Ignition is a direct consequence of both alpha heating and its feedback on the thermal energy and fusion-reaction rate. When this feedback process becomes unstable, it leads to a thermal runaway within the central hot spot.<sup>2</sup> A robustly ignited hot spot drives a burn wave in the surrounding dense shell, leading to fusion energy outputs in a megajoule range that greatly exceeds the thermal and kinetic energy supplied to the DT fuel by the implosion alone (~tens of kilojoules).

Recent experiments at the National Ignition Facility (NIF) (high-foot targets<sup>3</sup>) have demonstrated significant alpha heating using indirect drive (ID). To make progress toward ignition on the NIF,<sup>4</sup> it is crucial to be able to measure the level of alpha heating and to identify intermediate plasma states where the alpha heating is the leading source of input energy (alpha-dominated or burning plasmas). In magnetic confinement fusion (MCF),<sup>5</sup> the burning-plasma regime is identified through the thermonuclear  $Q = \text{fusion power output} / \text{external power input}$ . Since the alpha energy is about 1/5 of the total fusion energy, a  $Q = 5$  denotes the state where the alpha power equals the input power. For convenience, in this article we use  $Q_\alpha = \text{alpha power} / \text{input power} = Q/5$  and define the onset of a burning plasma at  $Q_\alpha = 1$  ( $Q = 5$ ).

While determining  $Q_\alpha$  for a steady-state MCF device is straightforward, the definition for ICF is greatly complicated

by the transient nature of an ICF implosion and by the fact that the vast majority of the input energy does not reach the DT plasma. Since this article is concerned only with the physics of burning plasmas and not with the prospects for fusion energy, the relevant input energy is the one reaching the DT plasma, where the fusion reactions occur. Therefore, the parameters  $Q$ ,  $Q_\alpha$  used here refer to the DT fuel and should not be confused with the engineering  $Q$  used for fusion reactors.<sup>5</sup>

Heating by the fusion alphas enhances the fusion yield to varying degrees, depending on the fraction of deposited alpha-particle energy to the total hot-spot energy. Here we consider yield amplifications  $\leq 10$ , which are of most interest for current implosions on the NIF and characteristic of a sub-ignited burning plasma. Using a simple model of the hot spot and shell dynamics (*alpha-heating model*), we find the burning-plasma conditions for ICF and show that the fusion-yield enhancement resulting from alpha heating depends only on the fractional alpha energy or the Lawson parameter<sup>6,7</sup> through a universal curve valid for direct- and indirect-drive ICF. It is shown that the alpha-heating model results are in good agreement with those from radiation-hydrodynamics simulations.

The alpha-heating model describes both the hot-spot formation and the piston action of the shell providing the external input energy. To correctly capture the  $PdV$  work to the hot spot and to the shell, the incompressible shell model<sup>7</sup> is not suitable; instead a compressible model similar to the one in Ref. 8 is used. In the final stage of the implosion, the shell is described as a compressible gas separated into two regions (shocked and free fall) by the return shock driven by the hot-spot pressure into the shell. The temporal evolution of the hydrodynamic quantities is determined from the beginning of the shell's deceleration phase up to the shell's rebound, and both the heat conduction and radiation losses are included. A fraction of the alpha particles escapes through the hot-spot boundary, depositing their energy into the cold shell and ablating shell mass into the hot spot. It is assumed that all of the radiation escapes from the hot spot, reducing the pressure and temperature. The fusion rate is approximated with  $\langle \sigma v \rangle \approx c_\alpha T^3$  ( $c_\alpha =$

const), which is sufficiently accurate in the interesting 4- to 8-keV range characteristic of a yield amplification  $\leq 10$ . The conservation equations for mass, momentum, and energy can be written in the dimensionless form:

$$\left(\hat{P}\hat{R}_h^3/\hat{T}\right)' = \hat{R}_h\hat{T}^{5/2} + 3/5(1-\theta_\alpha)\gamma\hat{P}^2\hat{R}_h^3, \quad (1)$$

$$\left(\hat{M}_{ss}\hat{U}_{ss}\right)' - \hat{M}_{ss}\hat{U}_{ff}(\hat{R}_k) = \hat{P}\hat{R}_h^2 + 2\int_{\hat{R}_h}^{\hat{R}_k}\hat{r}\hat{P}_{ss}d\hat{r}, \quad (2)$$

$$\hat{M}_{ss} = \hat{R}_k^2\hat{\rho}_{ff}(\hat{R}_k - \hat{U}_{ff}), \quad (3)$$

$$\hat{R}_k = 4/3\hat{U}_{ss}(\hat{R}_k) - 1/3\hat{U}_{ff}(\hat{R}_k), \quad (4)$$

$$\left(\hat{P}\hat{R}_h^5\right)' = \hat{P}^2\hat{R}_h^5(\gamma\hat{T} - \beta\hat{T}^{-3/2}). \quad (5)$$

Equation (1) is the hot-spot mass conservation used to infer the hot-spot temperature  $T$  with the right-hand side representing the mass ablation off the inner shell surface driven by the heat conduction<sup>7</sup> and alpha-particle losses.<sup>9</sup> Here  $\hat{R}_h$  represents the hot-spot radius. Equation (2) represents Newton's law for the shocked portion of the shell slowed down by the hot-spot pressure  $P$ . The return shock  $R_k$  separates the free-fall (ff) and the shocked (ss) regions of the shell. The shocked-shell pressure  $P_{ss}$  approximately varies linearly from the hot-spot pressure to the post-shock pressure given by the Rankine–Hugoniot (RH) relations. Equation (3) governs the shocked-shell mass and includes the flow of mass across the return shock. Equation (4) describes the evolution of the return-shock position  $R_k$  through the RH relations. The velocity within the shocked shell is determined through a Taylor expansion about the hot-spot radius using the isentropic relation of the shocked shell, leading to

$$\hat{U}_{ss}(\hat{r}) \approx \hat{R}_h + \left[\hat{R}_h/\hat{R}_h - (3/5)\hat{\phi}/\hat{\phi}\right](\hat{r} - \hat{R}_h), \quad (6)$$

where  $\hat{\phi} \equiv \hat{P}\hat{R}_h^5$ . Equation (5) is the hot-spot energy conservation where the two terms on the right-hand side represent the alpha-heating contribution and the radiation losses. The level of alpha heating and radiation losses are determined by the parameters  $\gamma$  and  $\beta$ , respectively. Some three-dimensional (3-D) effects resulting from the reduction of the hot-spot volume<sup>10</sup> from the deceleration-phase Rayleigh–Taylor spikes can be included through a clean volume analysis, as described in Ref. 7, but are omitted for simplicity in this article. Pressure, radius, and temperature are normalized with their stagnation

values  $T_s$ ,  $P_s$ , and  $R_s$  in the absence of alpha heating and radiation losses and for an incompressible shell with equal mass:

$$M_{sh}V_{imp}^2 = 4\pi P_s R_s^3, \quad (7)$$

$$\kappa_0 T_s^{7/2} = P_s R_s V_{imp}, \quad (8)$$

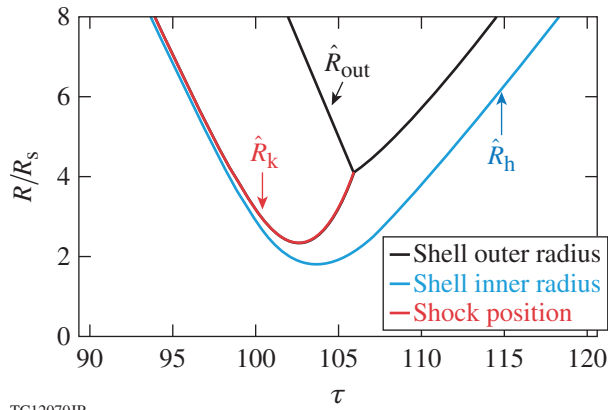
where  $V_{imp}$  is the implosion velocity,  $M_{sh}$  is the shell mass, and  $\kappa_0$  is the Spitzer thermal conductivity coefficient<sup>11</sup> in  $\kappa_{Sp} = \kappa_0 T^{5/2}$ . The dimensionless time is  $\tau = tV_{imp}/R_s$ . The dimensionless velocity is normalized with the peak implosion velocity  $V_{imp}$ . For simplicity we assume an initially uniform velocity profile so that  $\hat{U}_{ff} = -1$ . The dimensionless shocked-shell mass is defined as  $\hat{M}_{ss} = M_{ss}/M_{sh}$ . The dimensionless shell density is defined as  $\hat{\rho} = \rho/(M_{sh}/4\pi R_s^3)$  and its profile during the coasting phase (or free fall) is assumed to be approximately parabolic. The constant  $\gamma = c_\alpha \epsilon_\alpha P_s T_s R_s / (24 V_{imp})$  determines the level of alpha heating. The parameter  $\beta = c_b P_s R_s / (6T_s^{3/2} V_{imp})$  determines the radiation losses ( $c_b$  is the bremsstrahlung constant for the radiated power density  $\hat{P}_{rad} \approx c_b n^2 \sqrt{T}$ ). The fraction of escaping alphas is determined by analyzing Ref. 12:

$$\theta_\alpha(\xi_\alpha > 1/2) = 1 - 1/(4\xi_\alpha) + 1/(160\xi_\alpha^3), \quad (9)$$

$$\theta_\alpha(\xi_\alpha < 1/2) = 3/2\xi_\alpha - 4/5\xi_\alpha^2, \quad (10)$$

where  $\xi_\alpha = \xi_0 \hat{P}\hat{R}_h/\hat{T}^{5/2}$ . We use  $\xi_0 = 0.6$ , leading to a fraction of absorbed alphas at a bang time of about 0.7 to 0.8 in agreement with numerical simulations including alpha-transport physics. Equations (1)–(5) are solved from the beginning of the deceleration phase ( $t = 0$ ) with a radius much greater than the stagnation radius  $\hat{R}_h(0) = \hat{R}_0 \gg 1$ , a velocity equal to the implosion velocity  $\hat{R}_h'(0) = -1$ , and a very low initial pressure and temperature  $\hat{P}(0) = \hat{R}(0)^{-5/2}$ ,  $\hat{T}(0) = \hat{R}(0)^{-1/2}$ , respectively. At  $t = 0$ , the return shock is approaching the imploding shell [ $\hat{R}_k(0) = \hat{R}_0$ ] and the shocked-shell mass is zero [ $\hat{M}_{ss}(0) = 0$ ]. The initial aspect ratio is set to  $A_0 \approx 0.1\hat{R}_h(0)$ , leading to a stagnating mass of about 50% of the DT unablated mass as indicated by the hydrodynamic simulations of ignition targets.<sup>7</sup> Figure 142.1 shows the trajectories of the inner shell surface (or hot-spot radius), return shock, and outer shell surfaces. After the return shock reaches the outer surface, the entire shell mass is shocked and the shell behaves like a rigid piston.

The solution of Eqs. (1)–(5) exhibits a singularity (ignition) for a critical value of  $\gamma$  that depends on  $\beta$ . A numerical



TC12070JR

Figure 142.1

Trajectories from the model [Eqs. (1)–(5)] using  $\beta = 0$ ,  $\gamma = 0$ . The figure shows the time evolution of the hot-spot radius, the return shock inside the shell, and the shell's outer surface.

solution leads to the critical  $\gamma(\beta) \approx 28 + 4.3\beta + 2\beta^2$  for  $\beta \leq 2$ . The ignition parameter can be written as  $\chi_{\text{no } \alpha} = \gamma / \gamma(\beta)$  with  $\chi_{\text{no } \alpha} = 1$  being the ignition condition. From full hydrodynamic simulations with radiation on/off, we determine that radiation losses cause a reduction of  $\sim 15\%$  to  $20\%$  in hot-spot pressure and temperature, corresponding to a value of  $\beta \approx 1.5$  in the model [Eqs. (1)–(5)]. The subscript “no  $\alpha$ ” indicates that all the hydrodynamic quantities are evaluated without alpha-particle energy deposition ( $\gamma = 0$ ). Using Eqs. (7) and (8), both  $\gamma$  and  $\beta$  can be rewritten in terms of the shell's areal density and hot-spot temperature without alpha deposition. In one dimension (1-D), since both  $\gamma$  and  $\beta$  depend on areal density and temperature, the ignition parameter  $\chi_{\text{no } \alpha}$  also depends on areal density and temperature. Note that with respect to the incompressible thin-shell model of Ref. 7, the scaling of the ignition parameter is unchanged. A convenient form of  $\chi$  is written in terms of areal density and neutron yield:

$$\chi_{\text{no } \alpha} \simeq (\rho R_{\text{no } \alpha})^{0.61} \left( \frac{0.24 Y_{\text{no } \alpha}^{16}}{M_{\text{DT}}^{\text{unab}}} \right)^{0.34}, \quad (11)$$

where  $\rho R$  is in  $\text{g}/\text{cm}^2$ , yield is in  $10^{16}$ , and the unablated DT mass is in mg. Another form of  $\chi_{\text{no } \alpha}$  is given in Ref. 7:

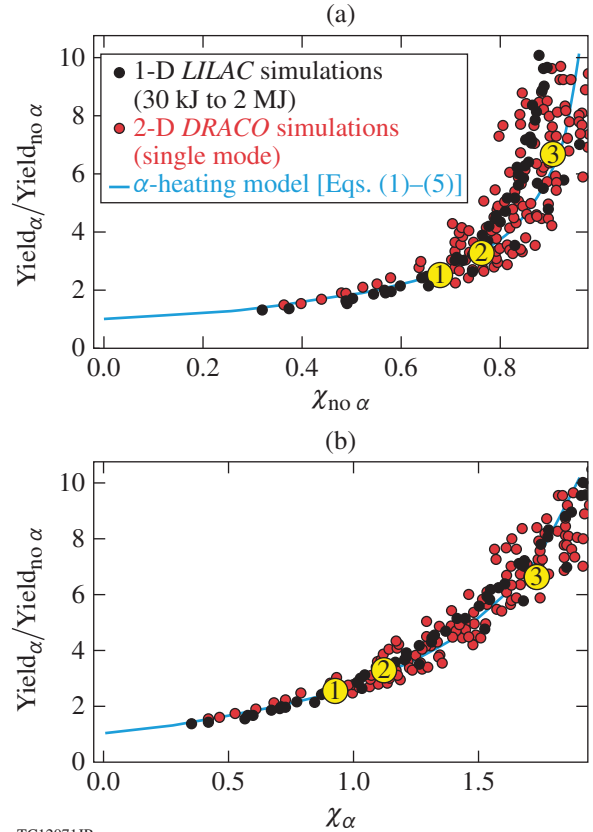
$$\chi_{\text{no } \alpha} \simeq (\rho R_{\text{no } \alpha})^{0.8} (T_{\text{no } \alpha} / 4.7)^{1.6} \text{YOC}_{\text{no } \alpha}^{0.4}, \quad (12)$$

where the temperature is in keV and the yield over clean (YOC)  $\equiv \text{yield}(3\text{-D})/\text{yield}(1\text{-D})$  is a measure of the level of nonuniformities in the implosion. The model [Eqs. (1)–(5)] is 1-D but the same clean-volume analysis of Ref. 7 can be applied to capture 3-D effects by redefining  $\chi$  as in Eq. (12), using the YOC, or

by using the measured yield in Eq. (11). Note that Eq. (11) can be derived from Eq. (12) by using the approximate formula for the 1-D yield  $Y_{16}(1\text{-D}) = \rho R^{0.56} (T/4.7)^{4.7} M_{\text{DT}} / 0.24$  (Ref. 7) into the YOC. The yield amplification caused by alpha heating is computed by solving Eqs. (1)–(5) with  $\gamma = 0$  (no alphas) and with a finite  $\gamma < \gamma(\beta)$  (i.e.,  $\chi_{\text{no } \alpha} < 1$ ). The ratio of the resulting fusion yields,

$$Y = \int_0^\infty \hat{P}^2 \hat{T} \hat{R}_h^3 d\tau,$$

represents the yield amplification. Figure 142.2(a) compares the yield amplification as a function of the ignition parameter obtained from hydrodynamic simulations with the curve from the alpha-heating model. The simulations were performed with the hydrocodes *LILAC* (1-D)<sup>13</sup> and *DRACO* (2-D).<sup>14</sup> The results can be approximated with the fitting formula



TC12071JR

Figure 142.2

Yield enhancement from alpha heating as a function of the alpha and no-alpha Lawson parameters using the model [Eqs. (1)–(5)] (solid curve) and hydrodynamic simulations (circles). The measurable parameter  $\chi_\alpha$  can be used to determine the yield amplification from (b). From this, (a) can be used to infer the no-alpha parameter  $\chi_{\text{no } \alpha}$ , which is useful to assess progress toward ignition. Points 1–3 represent simulations with mass and velocity similar to NIF indirect-drive (ID) targets (see Fig. 142.4).

$\hat{Y}_{\text{amp}} \approx (1 - \chi_{\text{no}\alpha}/0.96)^{-0.75}$ . As stated in Ref. 7, the  $\chi$ 's from Eqs. (11) and (12) are valid in 3-D for relatively fast targets with  $V_{\text{imp}} \sim 300$  to 400 km/s. Note that for a mass of DT of 0.18 mg,  $\chi_{\text{no}\alpha}^{2.9}$  is approximately equal to the experimental ignition threshold factor parameter<sup>15</sup> (ITFx) for the Livermore indirect-drive-ignition target,<sup>16</sup> indicating that the validity of Eq. (11) as an ignition parameter is also confirmed by a large database of indirect-drive ignition-target simulations. In experiments with significant alpha heating, the no- $\alpha$  quantities entering in the definition of  $\chi_{\text{no}\alpha}$  cannot be directly measured. The measured yield and areal density can still be used, however, in Eq. (11) to determine a value of  $\chi$  with alphas ( $\chi_{\alpha}$ ):

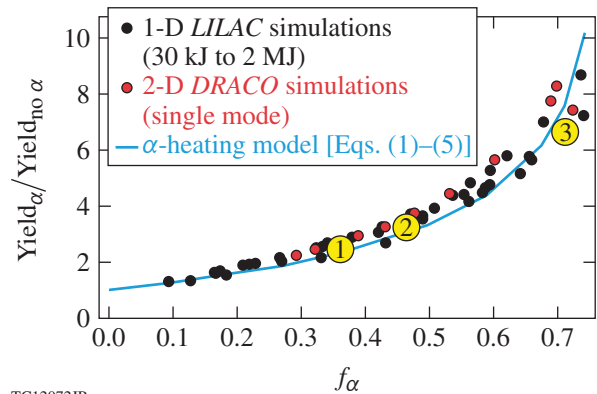
$$\chi_{\alpha} \approx (\rho R_{\alpha})^{0.61} \left( \frac{0.24 Y_{\alpha}^{16}}{M_{\text{DT}}^{\text{unab}}} \right)^{0.34}. \quad (13)$$

From Eqs. (1)–(5), a yield amplification curve using the measurable parameter  $\chi_{\alpha}$  has been generated [Fig. 142.2(b)]. The yield amplification is approximately a unique function of  $\chi_{\alpha}$ , indicating that inferring  $\chi_{\alpha}$  from the experimental observables ( $\rho R$  and yield) is sufficient to determine the yield amplification caused by alpha heating in an experiment. Figure 142.2(b) compares the yield amplification versus  $\chi_{\alpha}$  from simulations with the alpha-heating model [Eqs. (1)–(5)]. The model result can be approximated for amplifications  $\leq 10$  with the simple formula  $\hat{Y}_{\text{amp}} \approx \exp(\chi_{\alpha}^{1.2})$ . When compared to the results of Spears and Lindl<sup>17</sup> for the NIF indirect-drive-ignition target ( $M_{\text{DT}} \approx 0.18$  mg), the yield-amplification curves are in good agreement with the data points from the simulation database of that specific target. In Ref. 17, the Lawson parameter is computed from  $P\tau/(P\tau)_{\text{ign}}$  (related to  $\chi$  as in Ref. 7) with alpha deposition. In this article, the analysis is carried out in dimensionless form, and the results are applicable to all targets, large or small, direct drive or indirect drive, as long as the ignition parameter  $\chi_{\alpha}$  is calculated using Eq. (13). For the high-foot shot N140120 (Ref. 18), which achieved a yield of  $\sim 9.3 \times 10^{15}$  neutrons, an areal density of  $\approx 0.78$  g/cm<sup>2</sup>, and an ion temperature of 4.9 keV, with  $M_{\text{DT}} \approx 0.18$  mg, we find that  $\chi_{\alpha} \approx 0.92$  and the yield amplification is  $\sim 2.5$  (point 1 in Fig. 142.2), close to the simulation result.<sup>18</sup> The corresponding  $\chi_{\text{no}\alpha} \approx 0.66$  is inferred from Fig. 142.2.

A more-indicative measurable parameter for alpha heating is the fractional alpha energy ( $f_{\alpha}$ ) given by the ratio of the alpha energy deposited inside the hot spot up to bang time (peak of the neutron rate) and the neutron-averaged hot-spot energy

$$f_{\alpha} \equiv \frac{(1/2)\theta_{\alpha}E_{\alpha}}{(3/2)\langle P \rangle V_{\text{hs}}}. \quad (14)$$

This parameter is a direct measure of the importance of alpha heating to the hot-spot energy. The fractional alpha energy can be inferred directly from experimental observables, including hot-spot radius, ion temperature, neutron yield, and burnwidth. The alpha energy directly deposited up to bang time is about 1/2 of the total alpha energy times the absorbed fraction  $\theta_{\alpha}$ . The latter can be inferred using Eqs. (9) and (10) and  $\xi_{\alpha}$  from Ref. 12 (where  $\xi_{\alpha}$  is denoted with  $\tau$ ). The hot-spot energy can be inferred from its pressure  $\langle P \rangle$  and volume  $V_{\text{hs}}$  using the method in Ref. 19. Once the pressure is determined, the hot-spot density follows from the equation of state ( $\rho \sim P/T$ ); therefore, the absorbed alpha fraction is inferred from Ref. 12 using the hot-spot areal density and temperature. From the model [Eqs. (1)–(5)], one can reproduce the same quantities used in experiments to infer  $f_{\alpha}$ . Figure 142.3 shows the yield amplification from Eqs. (1)–(5) versus  $f_{\alpha}$  and compares it to the results of simulations using the same procedure to determine  $f_{\alpha}$  (as in an experiment). The two-dimensional (2-D) simulation results (red circles) require a lengthy post-processing analysis with the code *Spect3D*<sup>20</sup> to determine the x-ray-emitting volume measured in experiments.<sup>19</sup> Only a subset of the 2-D simulations in Fig. 142.2 has been post-processed. Figure 142.3 shows that the yield amplification is approximately a unique function of  $f_{\alpha}$ , which can also be used to infer the level of alpha heating. The yield amplification in Fig. 142.3 can be approximated by the simple formula  $\hat{Y}_{\text{amp}} \approx \exp[(f_{\alpha}/0.4)^{1.1}]$ . For the



TC12072JR  
Figure 142.3  
Yield enhancement caused by alphas versus the fractional alpha energy  $f_{\alpha}$ . Points 1–3 represent simulations with mass and velocity similar to current NIF ID targets (see Fig. 142.4).

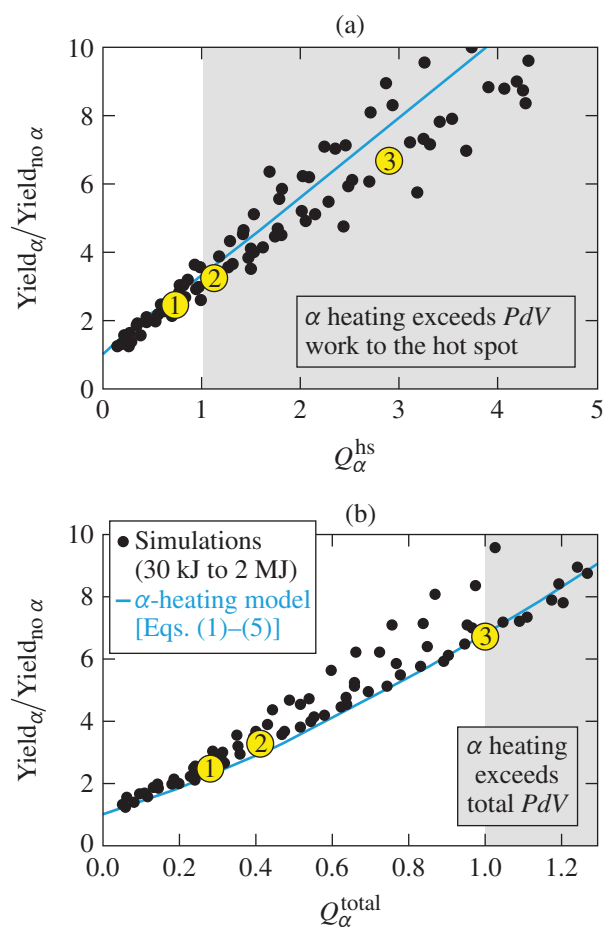
high-foot target N140120 (Ref. 18) (point 1 in Fig. 142.3), the fractional alpha energy is about 0.36 and the corresponding yield amplification of  $\approx 2.5$  is in agreement with the value obtained earlier through the  $\chi_\alpha$  method. The good agreement of the results from the alpha-heating model and the hydrodynamic simulations (Fig. 142.3) indicate that the model can be used to determine the input energy to the fusing plasma and, therefore, the onset of the burning-plasma regime. Energy is supplied to the DT plasma starting from the DT fuel's kinetic energy  $E_k(0) = 1/2 M_{\text{DT}} V_{\text{imp}}^2$ , where 0 is the beginning of the deceleration phase. Only a fraction of the kinetic energy is transformed into DT internal energy through the  $PdV$  work. At bang time, the kinetic energy converted to internal energy is  $E_{PdV}^{\text{tot}} = E_k(0) - E_k(t_{\text{bang}})$ . Of that fraction, a portion is transferred to the dense shocked shell ( $E_{PdV}^{\text{ss}}$ ) and the remainder to the hot spot ( $E_{PdV}^{\text{hs}}$ ). It is convenient to define two  $Q_\alpha$  parameters, one for the hot spot and one for the entire compressed core:

$$Q_\alpha^{\text{hs}} \equiv \frac{0.5E_\alpha}{E_{PdV}^{\text{hs}}}, \quad Q_\alpha^{\text{tot}} \equiv \frac{0.5E_\alpha}{E_{PdV}^{\text{tot}}}. \quad (15)$$

In these definitions, we retain the contribution of all the alpha particles up to bang time, including those that escape. The ablative flow carries the escaping alpha energy back into the hot spot and such energy is counted as input to the hot spot. The value  $Q_\alpha^{\text{hs}} > 1$  implies that the alpha heating exceeds the compression work to the hot spot and the hot-spot plasma enters the burning-plasma regime, where the alpha heating is the dominant heating mechanism. Additional  $PdV$  work is done on the shell itself as the return shock propagates outward and more shell material is slowed down and compressed. While few fusion reactions occur in the dense shell at yield amplifications below 10, the compressed shell provides the inertial confinement to the hot-spot pressure. The  $PdV$  work to the shell is not a direct input to the fusing plasma, but a highly compressed shell increases the confinement time and, therefore, the fusion yield of the hot spot. In the second definition of  $Q_\alpha$ , the total  $PdV$  work is included in the denominator and the condition  $Q_\alpha^{\text{tot}} > 1$  represents the regime where the alpha heating exceeds the total compression work. The  $PdV$  work to the hot spot can be calculated in 1-D from the integral

$$4\pi \int_{R(0)}^{R_{\text{stag}}} PR^2 dR,$$

where  $R_{\text{stag}}$  is the hot-spot stagnation radius. Both quantities can be computed from the model [Eqs. (1)–(5)] as well as from 1-D hydro simulations of the implosions. In 2-D and 3-D, extracting the  $PdV$  work is more complicated and will be addressed in a forthcoming article. Figure 142.4 shows the yield amplifications versus  $Q_\alpha^{\text{hs}}$  and  $Q_\alpha^{\text{tot}}$  and compares the result of the model [Eqs. (1)–(5)] with hydro simulations. From Fig. 142.4(a), the onset of the hot-spot burning-plasma regime occurs at yield amplifications of about 3.5. For current NIF ID implosions with  $M_{\text{DT}} \approx 0.18$  mg and fuel kinetic energies  $\sim 12$  to 15 kJ, this corresponds to a neutron yield of  $\sim 1.8 \times 10^{16}$



TC12073JR

Figure 142.4  
Plots of the yield amplification versus the hot-spot  $Q_\alpha$  and the total  $Q_\alpha$  from the model [Eqs. (1)–(5)] (solid curve) and from 1-D simulations (circles). The shaded areas identify the burning-plasma regimes. The three yellow circles (1–3) with yield amplification  $\sim 2.5\times$  [like shot N140120 (Ref. 19)],  $3.3\times$ , and  $6.7\times$  have a fuel kinetic energy of 12 to 15 kJ, and a DT mass  $\approx 0.18$  mg like current NIF ID experiments. Point 2 is located at the onset of hot-spot burning plasma. Point 3 is in the full burning-plasma regime.

(or  $\sim 50$  kJ) as indicated by point 2 in Fig. 142.4(a). The regime where the alpha heating exceeds the total  $PdV$  work occurs for yield amplifications  $\sim 7$ , corresponding to a yield  $\sim 4.5 \times 10^{16}$  (or  $\sim 120$  kJ) represented by point 3 in Fig. 142.4(b). The two measurable parameters  $f_\alpha$  and  $\chi_\alpha$  can be used to determine the onset of the burning-plasma regimes. Using Figs. 142.2 and 142.3, the hot-spot burning-plasma regime is achieved for  $f_\alpha \approx 0.45$  and  $\chi_\alpha \approx 1.2$ , while the full burning-plasma regime is achieved for  $f_\alpha \approx 0.7$  and  $\chi_\alpha \approx 1.8$ . The curves in Figs. 142.2–142.4 are used to assess the onset of the burning-plasma regime in ICF and the requirements on the implosion hydrodynamics to achieve ignition. For instance, the value  $\chi_{\text{no}\alpha} \approx 0.66$  for N140120 indicates that the no- $\alpha$  hydrodynamics must improve to raise the value of  $\chi_{\text{no}\alpha}$  by  $\geq 50\%$  to achieve ignition on the NIF.

## ACKNOWLEDGMENT

The authors thank Dr. J. Lindl, Dr. P. Patel, and Prof. D. Shvarts for many useful discussions. This work has been supported by the U.S. Department of Energy under Cooperative Agreement No. DE-FC02-04ER54789 (Fusion Science Center supported by the Office of Fusion Energy Sciences) and DE-NA0001944 (National Nuclear Security Administration), the New York State Energy Research Development Authority, and the University of Rochester. The support of DOE does not constitute an endorsement by DOE of the views expressed in this article.

## REFERENCES

1. J. Nuckolls *et al.*, *Nature* **239**, 139 (1972).
2. S. Atzeni and J. Meyer-ter-Vehn, *The Physics of Inertial Fusion: Beam Plasma Interaction, Hydrodynamics, Hot Dense Matter*, International Series of Monographs on Physics (Clarendon Press, Oxford, 2004); J. D. Lindl, *Inertial Confinement Fusion: The Quest for Ignition and Energy Gain Using Indirect Drive* (Springer-Verlag, New York, 1998).
3. O. A. Hurricane *et al.*, *Nature* **506**, 343 (2014).
4. M. J. Edwards, P. K. Patel, J. D. Lindl, L. J. Atherton, S. H. Glenzer, S. W. Haan, J. D. Kilkenny, O. L. Landen, E. I. Moses, A. Nikroo, R. Petrasso, T. C. Sangster, P. T. Springer, S. Batha, R. Benedetti, L. Bernstein, R. Betti, D. L. Bleuel, T. R. Boehly, D. K. Bradley, J. A. Caggiano, D. A. Callahan, P. M. Celliers, C. J. Cerjan, K. C. Chen, D. S. Clark, G. W. Collins, E. L. Dewald, L. Divol, S. Dixit, T. Doepfner, D. H. Edgell, J. E. Fair, M. Farrell, R. J. Fortner, J. Frenje, M. G. Gatu Johnson, E. Giraldez, V. Yu. Glebov, G. Grim, B. A. Hammel, A. V. Hamza, D. R. Harding, S. P. Hatchett, N. Hein, H. W. Herrmann, D. Hicks, D. E. Hinkel, M. Hoppe, W. W. Hsing, N. Izumi, B. Jacoby, O. S. Jones, D. Kalantar, R. Kauffman, J. L. Kline, J. P. Knauer, J. A. Koch, B. J. Koziolowski, G. Kyrala, K. N. LaFortune, S. Le Pape, R. J. Leeper, R. Lerche, T. Ma, B. J. MacGowan, A. J. MacKinnon, A. MacPhee, E. R. Mapoles, M. M. Marinak, M. Mauldin, P. W. McKenty, M. Meezan, P. A. Michel, J. Milovich, J. D. Moody, M. Moran, D. H. Munro, C. L. Olson, K. Opachich, A. E. Pak, T. Parham, H.-S. Park, J. E. Ralph, S. P. Regan, B. Remington, H. Rinderknecht, H. F. Robey, M. Rosen, S. Ross, J. D. Salmonson, J. Sater, D. H. Schneider, F. H. Séguin, S. M. Sepke, D. A. Shaughnessy, V. A. Smalyuk, B. K. Spears, C. Stoeckl, W. Stoeffl, L. Suter, C. A. Thomas, R. Tommasini, R. P. Town, S. V. Weber, P. J. Wegner, K. Widman, M. Wilke, D. C. Wilson, C. B. Yeamans and A. Zylstra, *Phys. Plasmas* **20**, 070501 (2013).
5. J. P. Freidberg, *Plasma Physics and Fusion Energy* (Cambridge University Press, Cambridge, England, 2007).
6. J. D. Lawson, *Proc. Phys. Soc. Lond. B* **70**, 6 (1957).
7. P. Y. Chang, R. Betti, B. K. Spears, K. S. Anderson, J. Edwards, M. Fatenejad, J. D. Lindl, R. L. McCrory, R. Nora, and D. Shvarts, *Phys. Rev. Lett.* **104**, 135002 (2010); R. Betti, P. Y. Chang, B. K. Spears, K. S. Anderson, J. Edwards, M. Fatenejad, J. D. Lindl, R. L. McCrory, R. Nora, and D. Shvarts, *Phys. Plasmas* **17**, 058102 (2010).
8. R. Betti, K. Anderson, V. N. Goncharov, R. L. McCrory, D. D. Meyerhofer, S. Skupsky, and R. P. J. Town, *Phys. Plasmas* **9**, 2277 (2002).
9. A. Schiavi and S. Atzeni, *Phys. Plasmas* **14**, 070701 (2007).
10. R. Kishony and D. Shvarts, *Phys. Plasmas* **8**, 4925 (2001).
11. L. Spitzer, *Physics of Fully Ionized Gases* (Interscience Publishers, New York, 1956).
12. O. N. Krokhin and V. B. Rozanov, *Sov. J. Quantum Electron.* **2**, 393 (1973).
13. J. Delettrez, R. Epstein, M. C. Richardson, P. A. Jaanimagi, and B. L. Henke, *Phys. Rev. A* **36**, 3926 (1987).
14. P. B. Radha, T. J. B. Collins, J. A. Delettrez, Y. Elbaz, R. Epstein, V. Yu. Glebov, V. N. Goncharov, R. L. Keck, J. P. Knauer, J. A. Marozas, F. J. Marshall, R. L. McCrory, P. W. McKenty, D. D. Meyerhofer, S. P. Regan, T. C. Sangster, W. Seka, D. Shvarts, S. Skupsky, Y. Srebro, and C. Stoeckl, *Phys. Plasmas* **12**, 056307 (2005).
15. B. K. Spears *et al.*, *Phys. Plasmas* **19**, 056316 (2012).
16. S. W. Haan, J. D. Lindl, D. A. Callahan, D. S. Clark, J. D. Salmonson, B. A. Hammel, L. J. Atherton, R. C. Cook, M. J. Edwards, S. Glenzer, A. V. Hamza, S. P. Hatchett, M. C. Herrmann, D. E. Hinkel, D. D. Ho, H. Huang, O. S. Jones, J. Kline, G. Kyrala, O. L. Landen, B. J. MacGowan, M. M. Marinak, D. D. Meyerhofer, J. L. Milovich, K. A. Moreno, E. I. Moses, D. H. Munro, A. Nikroo, R. E. Olson, K. Peterson, S. M. Pollaine, J. E. Ralph, H. F. Robey, B. K. Spears, P. T. Springer, L. J. Suter, C. A. Thomas, R. P. Town, R. Vesey, S. V. Weber, H. L. Wilkens, and D. C. Wilson, *Phys. Plasmas* **18**, 051001 (2011).
17. B. K. Spears and J. D. Lindl, "Ignition Metrics and Their Role in Setting Specifications and Evaluating Progress Toward Ignition on the NIF," Lawrence Livermore National Laboratory, Livermore, CA (internal report, unpublished).
18. O. A. Hurricane, D. A. Callahan, D. T. Casey, E. L. Dewald, T. R. Dittrich, T. Döppner, M. A. Barrios Garcia, D. E. Hinkel, L. F. Berzak Hopkins, P. Kervin, J. L. Kline, S. Le Pape, T. Ma, A. G. MacPhee, J. L. Milovich, J. Moody, A. E. Pak, P. K. Patel, H.-S. Park, B. A. Remington, H. F. Robey, J. D. Salmonson, P. T. Springer, R. Tommasini, L. R. Benedetti, J. A. Caggiano, P. Celliers, C. Cerjan, R. Dylla-Spears, D. Edgell, M. J. Edwards, D. Fittinghoff, G. P. Grim, N. Guler, N. Izumi, J. A. Frenje, M. Gatu Johnson, S. Haan, R. Hatarik, H. Herrmann, S. Khan, J. Knauer, B. J. Koziolowski, A. L. Kritcher, G. Kyrala, S. A. Maclaren, F. E. Merrill, P. Michel, J. Ralph, J. S. Ross, J. R. Rygg, M. B. Schneider, B. K. Spears, K. Widmann, and C. B. Yeamans, *Phys. Plasmas* **21**, 056314 (2014).
19. C. Cerjan, P. T. Springer, and S. M. Sepke, *Phys. Plasmas* **20**, 056319 (2013).
20. J. J. MacFarlane *et al.*, *High Energy Density Phys.* **3**, 181 (2007).